

 Open access • Posted Content • DOI:10.1101/2021.04.19.440480

## Triggered reversible disassembly of an engineered protein nanocage

— [Source link](#) 

Jesse A. Jones, Ajitha S. Cristie-David, Michael P. Andreas, Tobias W. Giessen

**Institutions:** University of Michigan

**Published on:** 19 Apr 2021 - bioRxiv (Cold Spring Harbor Laboratory)

Related papers:

- [Triggered Reversible Disassembly of an Engineered Protein Nanocage](#)
- [Advances in encapsulin nanocompartment biology and engineering.](#)
- [Engineered protein and protein-polysaccharide cages for drug delivery and therapeutic applications](#)
- [Rational Design of Supramolecular Dynamic Protein Assemblies by Using a Micelle-Assisted Activity-Based Protein-Labeling Technology.](#)
- [Multifunctional DNA nanomaterials for biomedical applications](#)

Share this paper:    

View more about this paper here: <https://typeset.io/papers/triggered-reversible-disassembly-of-an-engineered-protein-b1uds8a1kz>

# 1 **Triggered reversible disassembly of an engineered protein nanocage**

2 Jesse A. Jones<sup>#</sup>, Ajitha S. Cristie-David<sup>#</sup>, Michael P. Andreas, and Tobias W. Giessen\*

3 Department of Biomedical Engineering, University of Michigan Medical School, Ann Arbor, MI, USA

4 Department of Biological Chemistry, University of Michigan Medical School, Ann Arbor, MI, USA

5 \*correspondence: [tgiessen@umich.edu](mailto:tgiessen@umich.edu)

## 6 **Abstract**

7 Protein nanocages play crucial roles in sub-cellular compartmentalization and spatial control in all  
8 domains of life and have been used as biomolecular tools for applications in biocatalysis, drug  
9 delivery, and bionanotechnology. The ability to control their assembly state under physiological  
10 conditions would further expand their practical utility. To gain such control, we introduced a peptide  
11 capable of triggering conformational change at a key structural position in the largest known  
12 encapsulin nanocompartment. We report the structure of the resulting engineered nanocage and  
13 demonstrate its ability to on-demand disassemble and reassemble under physiological conditions.  
14 We demonstrate its capacity for *in vivo* encapsulation of proteins of choice while also demonstrating  
15 *in vitro* cargo loading capabilities. Our results represent a functionally robust addition to the  
16 nanocage toolbox and a novel approach for controlling protein nanocage disassembly and  
17 reassembly under mild conditions.

## 18 Introduction

19 Intracellular compartmentalization is an effective strategy employed by all organisms to regulate  
20 metabolism and achieve spatial control.<sup>1,2</sup> One widespread compartmentalization approach is the  
21 use of protein nanocages. They can accumulate and store labile compounds, sequester toxic or  
22 volatile reaction intermediates, and prevent undesired side reactions of encapsulated enzymes.<sup>1,2</sup>  
23 Efforts have been undertaken to engineer protein nanocages like ferritins, lumazine synthase, and  
24 virus-like particles for various biomedical and industrial applications,<sup>3-5</sup> but few have focused on  
25 engineering input-responsive nanostructures capable of triggered assembly or disassembly.<sup>6,7</sup> Such  
26 controllable structures would expand the potential application range of engineered nanocages to  
27 include programmable delivery of encapsulated payloads and rationally timed substrate-product  
28 release and intermixing, to name only a few examples. Encapsulin nanocompartments have recently  
29 emerged as a particularly versatile bioengineering tool, resulting in their application as  
30 bionanoreactors, targeted delivery systems, and nano- and biomaterials production platforms.<sup>8-11</sup>

31 Encapsulins are icosahedral protein nanocages found in bacteria and archaea with triangulation  
32 numbers of T=1 (24 nm), T=3 (32 nm) or T=4 (42 nm) containing sub-nanometer pores at the  
33 symmetry axes.<sup>12</sup> They self-assemble from a single HK97-fold capsid protein into 60mer (T=1),  
34 180mer (T=3) or 240mer (T=4) protein cages and are involved in oxidative stress resistance,<sup>13-16</sup> iron  
35 mineralization and storage,<sup>17,18</sup> and sulfur metabolism.<sup>19</sup> Their defining feature is the ability to  
36 encapsulate dedicated cargo proteins via short C-terminal targeting peptides (TPs) found in cargo  
37 proteins which specifically interact with the interior of the protein shell during self-assembly.<sup>16,20,21</sup>  
38 This native feature has been reliably coopted for the facile encapsulation of non-native proteins  
39 through TP-fusions.<sup>22</sup>

40 Once assembled, encapsulins exhibit notable robustness and stability.<sup>23,24</sup> While often a desirable  
41 characteristic, this also precludes their easy disassembly under physiological conditions, a key  
42 feature for responsive delivery systems, nanoreactors, and biomaterials. In particular, encapsulins'  
43 inherent stability prevents efficient release of molecules synthesized in their interior, cargo enzyme  
44 "hot-swapping" for sequential packaging, or triggered cargo release for drug delivery applications.

45 Here we develop an engineered protein nanocage based on a bacterial encapsulin that exhibits  
46 triggered reversible disassembly under physiological conditions while also maintaining cargo loading  
47 capabilities.

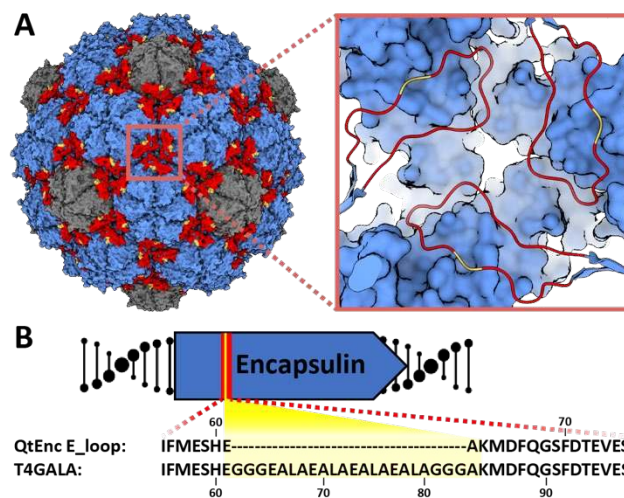
## 48 Results and Discussion

### 49 Protein cage selection and design of the disassembly trigger

50 The T=4 *Quasibacillus thermotolerans* encapsulin (QtEnc) was chosen as an engineering scaffold.  
51 QtEnc is the largest bacterial encapsulin known to date and is comprised of a thermostable, non-  
52 covalent chainmail formed from a single self-assembling protomer. Additionally, QtEnc is easily  
53 overexpressed and purified from *Escherichia coli* in an empty or cargo-loaded state.<sup>18</sup> QtEnc was  
54 analyzed for engineerable structural features important for protein cage assembly that might also be  
55 tolerant to mutation, and would not interfere with cargo loading. We chose to focus on the  
56 elongated loop (E-loop) region of the encapsulin protein which makes critical intra- and inter-  
57 capsomer contacts and influences overall shell topology (**Figure 1A**).<sup>18</sup> The E-loop is also located

58 away from the N-terminal helix important for cargo loading.<sup>25</sup> Therefore, the E-loop was selected as  
59 the insertion site for the disassembly trigger.

60 The GALA peptide has been shown to demonstrate an inducible coil-to-helix conformational change  
61 upon acidification<sup>6,26</sup> and was chosen as a disassembly trigger. A 16-residue GALA peptide flanked by  
62 triple glycine linkers was inserted between QtEnc residues Glu61 and Ala62 yielding the engineered  
63 nanocage T4GALA (**Figure 1B; Figure S1, TableS1**). We hypothesized that under neutral and basic  
64 conditions, the GALA peptide random coil would not disturb E-loop conformation or shell assembly.  
65 Upon acidification, the GALA coil would be expected to adopt a helical conformation and introduce  
66 enough torsional strain to disrupt critical E-loop contacts, thereby perturbing structural integrity  
67 enough to induce disassembly of the protein cage. A reversion of the GALA helix back to its relaxed  
68 random coil state under less acidic conditions would be expected to allow reassembly of the  
69 encapsulin cage.



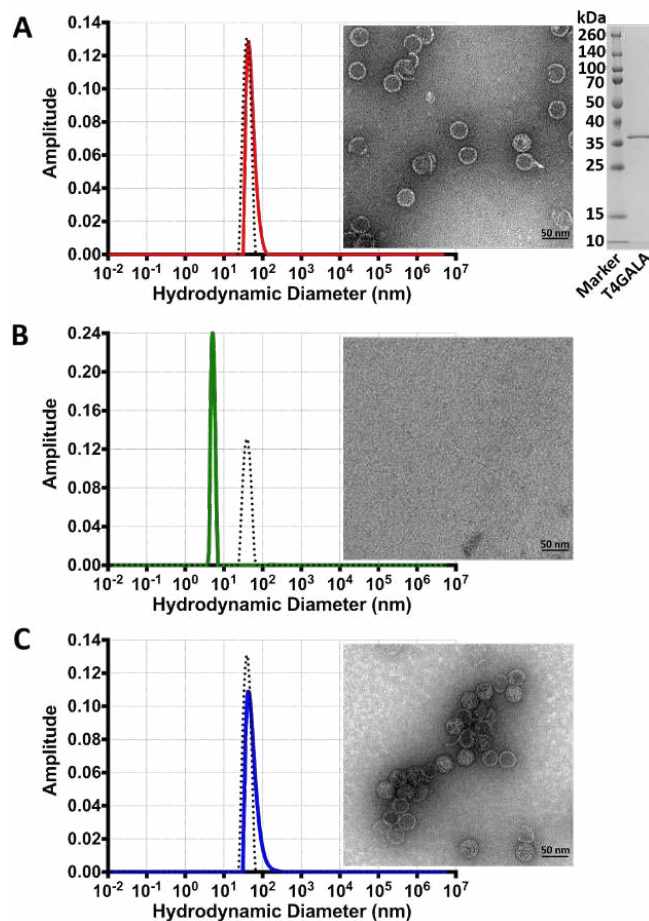
70

71 **Figure 1.** Design of the engineered protein nanocage. A) Surface view of the native *Quasibacillus thermotolerans* T4  
72 encapsulin (QtEnc, PDB 6NJ8), highlighting hexameric (blue) and pentameric (gray) facets, and E-loops (red) along with the  
73 GALA peptide insertion site (yellow). Inset: zoomed-in view of the three-fold symmetry axis and insertion site. B) E-loop  
74 (red) sequence of QtEnc and T4GALA highlighting the GALA insertion (yellow).

### 75 Assembly, disassembly, and reassembly of T4GALA

76 To characterize the engineered nanocage, C-terminally His-tagged T4GALA was expressed and  
77 purified using Ni-NTA resin and found to still assemble via transmission electron microscopy (TEM)  
78 analysis (**Figure 2A**). Native polyacrylamide gel electrophoresis (PAGE) studies were then conducted  
79 to analyze the effects of pH, salt, and buffer on the engineered protein cage (**Figure S2**). T4GALA  
80 exhibited a tendency for disassembly at low pH, with near-complete disassembly achieved at pH 6.0.  
81 An unexpected dependence of T4GALA structural integrity on buffer identity was also observed.  
82 Specifically, disassembly at physiological pH was favored in the presence of Tris buffer (pH 7.5) while  
83 Bis-tris propane was found to significantly stabilize T4GALA under similar pH conditions.

84 Size exclusion chromatography (SEC) showed that the elevated imidazole concentrations used for Ni-  
85 NTA elution helped maintain T4GALA in an assembled state even in Tris buffer. Imidazole was added  
86 to SEC buffers for all subsequent purifications (**Figure S3**). As such, T4GALA is easily overexpressed in  
87 *E. coli* and purified in the assembled state via a simple two-step protocol.



88

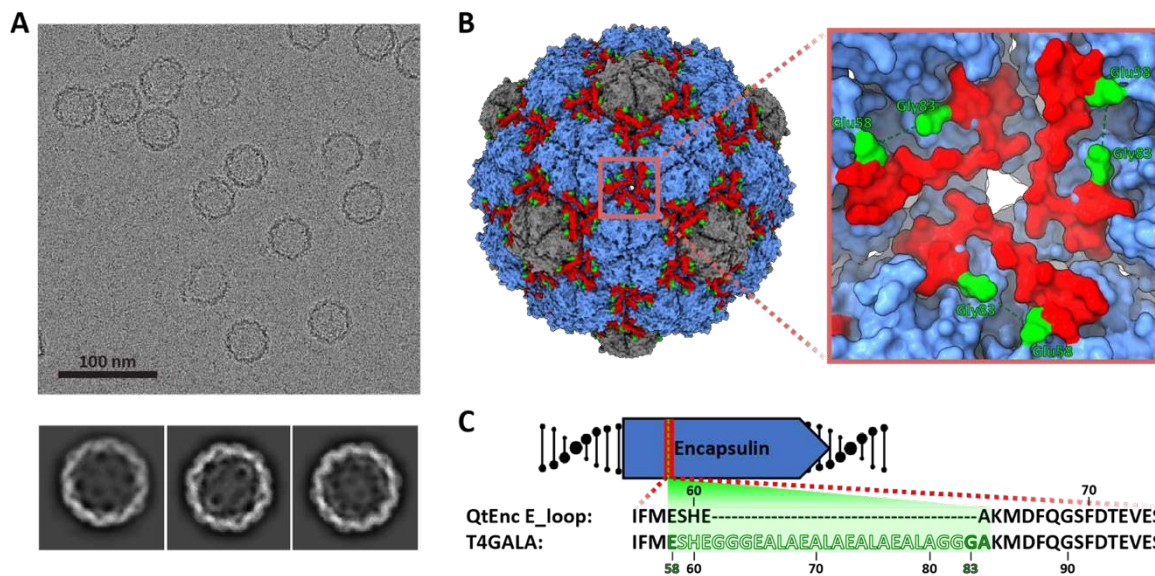
89 **Figure 2.** Assembly, disassembly, and reassembly of the T4GALA protein cage. A) Dynamic light scattering analysis (left) of  
90 assembled T4GALA (red) compared to native QtEnc (black dashed) with assembled T4GALA verified via TEM (right). SDS-  
91 PAGE analysis of purified T4GALA (far right). B) DLS analysis (left) of disassembled T4GALA after centrifugation (green) with  
92 QtEnc reference (black dashed) and disassembled T4GALA TEM analysis (right). C) DLS analysis (left) of reassembled  
93 T4GALA (blue) with QtEnc reference (black dashed) and reassembled T4GALA TEM analysis (right). Scale bars: 50 nm.

94 As concern existed regarding the potential for prolonged exposure to Tris buffer and unfavorable pH  
95 conditions during native PAGE analysis, assembly states were verified and characterized by a more  
96 reliable combination of dynamic light scattering (DLS) analysis and TEM (**Figure 2, Figure S4**). A  
97 streamlined protocol was developed to purify T4GALA via standard Ni-NTA conditions, disassembly  
98 in imidazole-free Tris buffer, and reassembly in Bis-tris propane, all under physiological pH  
99 conditions. Overall, assembled T4GALA proved to be similar to native QtEnc in size (QtEnc Z-average  
100 diameter 47.2 nm, peak diameter 43.4 nm; T4GALA Z-average diameter 62.2 nm, peak diameter  
101 56.39 nm) and monodisperse (**Figure 2A**), with the slight increase in average diameter by DLS  
102 possibly due to the additional disordered insert and potential small lipophilic aggregates. After brief  
103 centrifugation, the disassembled sample appears monodisperse with a diameter of ~6 nm (Z-average  
104 diameter 6.8 nm, peak diameter 5.4 nm) (**Figure 2B**). Upon reassembly, T4GALA re-forms mostly  
105 monodisperse protein cages of the expected diameter (Z-average diameter 76.78 nm, peak diameter  
106 55.31 nm), with a slight increase in aggregation observed by TEM and DLS analysis. (**Figure 2C**).

107 Structural characterization of the T4GALA protein nanocage

108 To further characterize T4GALA, cryogenic electron microscopy (cryo-EM) was carried out on the  
109 engineered protein cage. The overall structure of T4GALA shows that it self-assembles into a 7.7

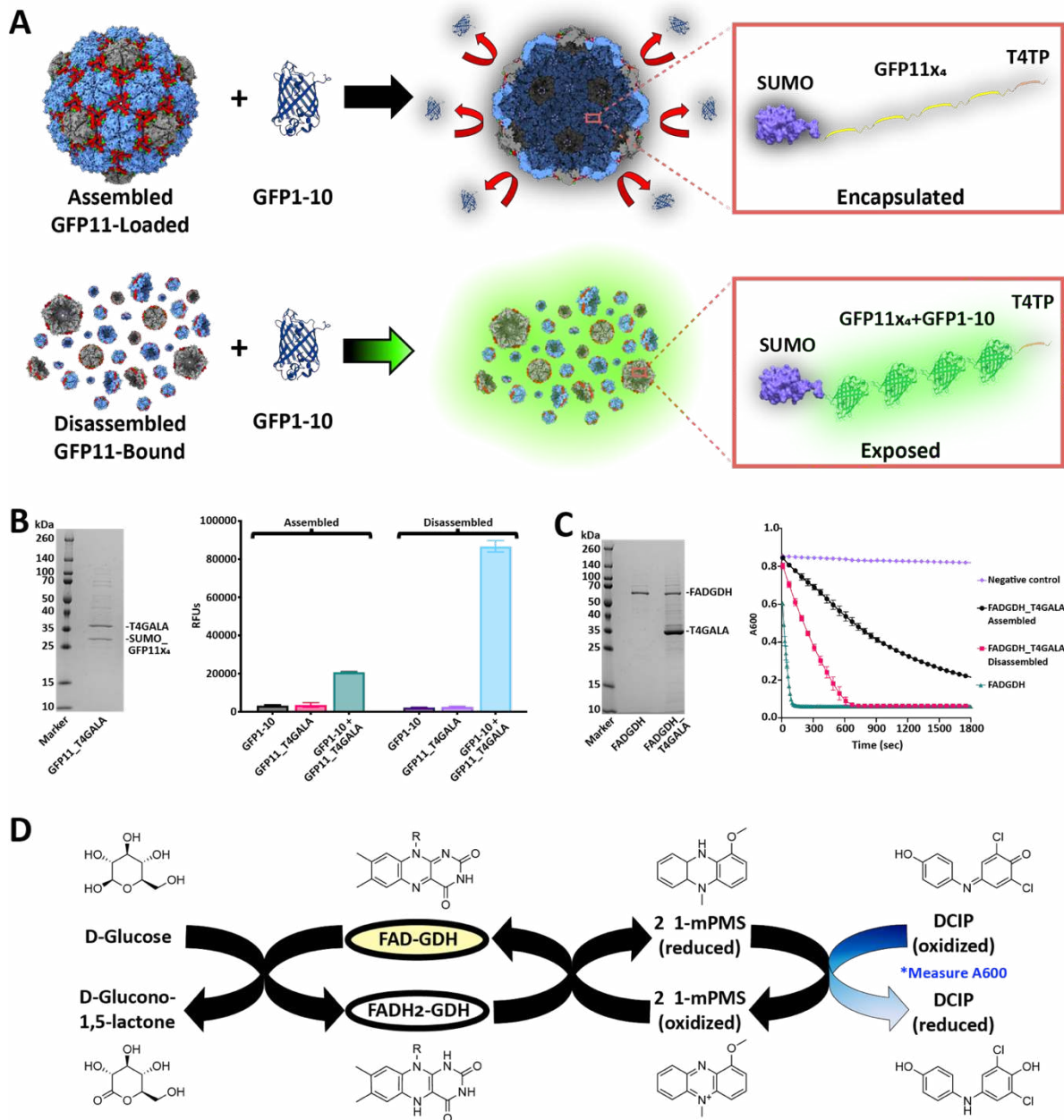
110 MDa 240mer (T=4) nanocompartment about 42 nm in diameter, nearly identical to native QtEnc  
 111 (PDB 6NJ8). However, T4GALA exhibits a notable absence of cryo-EM density in the E-loop region  
 112 between residues Glu58 and Gly83, corresponding to the GALA insertion site (**Figure 3, Figure S5,**  
 113 **Figure S6, Table S2**). Specifically, E-loops at the three-fold symmetry axis formed by three  
 114 neighboring hexameric capsomers show no density for 21 out of 22 GALA insertion residues –  
 115 including the glycine linkers. Three additional residues (Glu58, Ser59, and His60) preceding the GALA  
 116 insertion site lack density as well. At the pseudo-three-fold axis formed by two hexameric and one  
 117 pentameric capsomer, a similar absence of density is observed around the GALA insertion site  
 118 (**Figure S7**). While density is visible for all other E-loop residues, model-to-map correlation is  
 119 relatively low for these E-loop residues across different chains (**Figure S8**), suggesting the engineered  
 120 E-loop is more structurally dynamic, corroborating the goal of creating a less structurally rigid,  
 121 triggerable E-loop.



122  
 123 **Figure 3.** Structural analysis of T4GALA. A) Representative motion-corrected electron cryomicrograph (top) and 2D class  
 124 averages of T4GALA. B) Cryo-EM density of T4GALA. Hexameric and pentameric capsomers shown in blue and grey,  
 125 respectively. E-loops are highlighted in red and the last visible residues flanking the GALA insertion site are shown in green  
 126 (Glu58 and Gly83). Inset (right) highlighting details of the three-fold symmetry axis to emphasize missing E-loop density  
 127 (Ser59 to Gly82, green dashes). C) Schematic highlighting the observed (solid) and missing (silhouette) residues in the  
 128 T4GALA E-loop.

### 129 *In vivo* cargo loading of T4GALA, cargo sequestration, and cargo activity

130 An N-terminally sumoylated quadruple tandem repeat split fluorescent protein (sFP) was fused at  
 131 the C-terminus to a QtEnc targeting peptide (T4TP) and cloned immediately upstream of the T4GALA  
 132 gene for co-expression (**Figure 4A**).<sup>18,27,28</sup> *In vivo* cargo loading capabilities were then confirmed via  
 133 Ni-NTA affinity co-purification (**Figure 4B**). Additionally, plate-based sFP complementation  
 134 fluorescence analysis further confirmed *in vivo* cargo loading while also confirming triggered  
 135 disassembly capabilities (**Figure 4A, 4B**).<sup>29</sup> Assembled GFP11x<sub>4</sub>-loaded and disassembled GFP11x<sub>4</sub>-  
 136 bound T4GALA were individually mixed with separately purified GFP1-10 sFP complement and each



137

138 **Figure 4.** *In vivo* cargo loading of T4GALA and characterization of cargo-loaded systems. A) Schematic of split fluorescent  
 139 protein experiments. Assembled (top) and disassembled (bottom) GFP11<sub>x4</sub>-loaded/bound T4GALA exposed to the GFP1-10  
 140 complement. B) SDS-PAGE analysis of GFP11<sub>x4</sub>-loaded T4GALA (left). Plate-based fluorescence assays (right) showing increased  
 141 relative fluorescence for disassembled GFP11<sub>x4</sub>-bound T4GALA complementation (light blue; right) compared to roughly four-  
 142 fold lower fluorescence for an equimolar amount of assembled GFP11<sub>x4</sub>-loaded T4GALA (green, left). C) SDS-PAGE analysis of  
 143 GDH and GDH-loaded T4GALA (left). Plate-based assays (right) comparing enzymatic activity of unencapsulated FAD-dependent  
 144 glucose dehydrogenase enzyme (green triangles), *in vivo* T4GALA-encapsulated enzyme in the assembled state (black squares),  
 145 and *in vivo* T4GALA-encapsulated enzyme in the disassembled state (pink squares) with buffer blank as a negative control  
 146 (purple diamonds). Data are shown as means while error bars represent standard deviations from three independent  
 147 experiments. D) Schematic summary of the catalyzed enzymatic reaction and the complementary assay measuring the resultant  
 148 decrease in absorption at 600 nm as DCIP is reduced. FAD, flavin adenine dinucleotide; GDH, glucose dehydrogenase; 1-mPMS,  
 149 1-methoxy-5-methylphenazinium methylsulfate; DCIP, 2,6-dichloroindophenol.

150

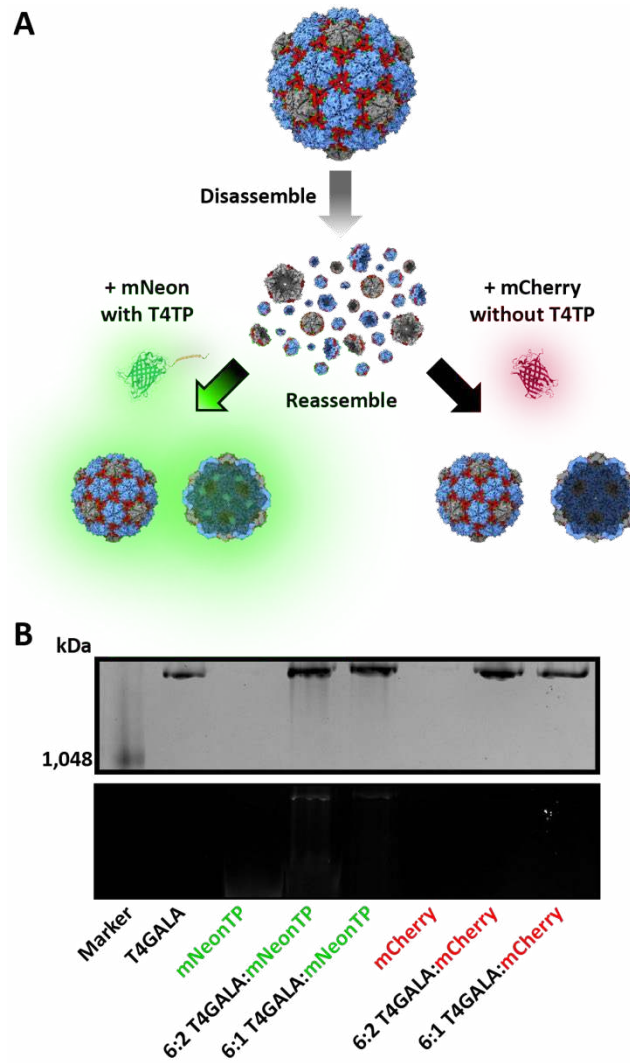


151 separate reaction was allowed to mature overnight for 16 hours. Assembled T4GALA prevented the  
152 encapsulated GFP11x<sub>4</sub> from interacting with GFP1-10 resulting in low relative fluorescence as  
153 compared to disassembled T4GALA, which allowed for robust GFP1-10 complementation yielding  
154 more than four-fold relative fluorescence. The ability of T4GALA to create a sequestered nanoscale  
155 space and robustly encapsulate its cargo until purposefully triggering disassembly will be a useful  
156 feature for various biomolecular engineering applications.

157 To expand the characterization of *in vivo* loading to enzymes and test potential diffusion barrier  
158 effects of encapsulation, a T4 targeting peptide was fused to the C-terminus of a flavin adenine  
159 dinucleotide-dependent glucose dehydrogenase enzyme (GDH),<sup>30</sup> cloned immediately upstream of  
160 T4GALA, and co-expressed for *in vivo* encapsulation. Cargo loading capabilities were again confirmed  
161 via Ni-NTA affinity co-purification and time-course analyses were conducted via the 2,6-  
162 dichloroindophenol (DCIP) assay, which monitors the decrease in absorbance at 600 nm as DCIP is  
163 reduced, to determine whether GDH loaded into T4GALA *in vivo* could maintain enzymatic activity  
164 (**Figure 4C and 4D**).<sup>30,31</sup> Comparisons were therefore made between equimolar amounts of free GDH  
165 enzyme, encapsulated GDH, and GDH enzyme bound to disassembled T4GALA. While T4GALA-  
166 encapsulated GDH exhibited enzymatic activity, the free enzyme displayed substantially faster  
167 kinetics. Upon disassembly, the reaction rate increased substantially, but was still observed to be  
168 slower than free GDH. It is widely reported throughout the literature that enzymes tethered to a  
169 surface often display decreased specific activity,<sup>32</sup> and it has also been reported that encapsulated  
170 enzymes often exhibit decreased specific activity, hypothesized to be the result of rapid *in vivo*  
171 encapsulation which may prevent proper folding and cofactor binding.<sup>33</sup> Additionally, the protein  
172 shell likely acts as a diffusion barrier which may decrease the flux of certain substrates and products  
173 in and out of the protein nanocage. Therefore, a decrease in encapsulated enzyme activity such as  
174 that observed here is not wholly unanticipated. Overall, the *in vivo* encapsulation of an active  
175 enzyme, along with its maintained activity after disassembly, highlights the potential modularity and  
176 applicability of the T4GALA system.

#### 177 *In vitro* cargo loading of T4GALA

178 To analyze whether the engineered T4GALA protein cage is capable of being disassembled, loaded *in*  
179 *vitro* with exogenous cargo, and then reassembled, a T4 targeting peptide was fused to the C-  
180 terminus of mNeonGreen fluorescent protein (mNeonTP). After disassembly of T4GALA, it was  
181 mixed with the separately expressed and purified mNeonTP in different molar ratios (6:2 and 6:1  
182 T4GALA:mNeonTP) and then incubated overnight to allow complementation and maturation (**Figure**  
183 **5A**). Next, T4GALA was reassembled and assessed for *in vitro* cargo loading via native PAGE and  
184 fluorescence analysis (**Figure 5b, Figure S9**). Fluorescence of the loaded mNeonTP was observed  
185 along with the high molecular weight reassembled T4GALA protein band, suggesting the engineered  
186 protein cage is capable of being loaded with exogenous cargo *in vitro*. Importantly, the experiment  
187 was conducted in parallel with an alternative mCherry fluorescent protein lacking the T4 targeting  
188 peptide as a negative control. The negative control sample failed to exhibit *in vitro* T4GALA  
189 encapsulation, indicated by a lack of co-migrating fluorescence during native PAGE analysis. The  
190 ability to easily encapsulate proteins inside a defined protein shell under mild conditions *in vitro*  
191 once again highlights the potential broad application range of the T4GALA system.



192

193 **Figure 5.** *In vitro* cargo loading of T4GALA. A) Schematic of T4GALA *in vitro* cargo loading including protein cage  
194 disassembly, *in vitro* loading of targeting peptide-fused cargo (left) and T4GALA reassembly resulting in detectable  
195 fluorescence from newly encapsulated mNeon cargo. Conversely, the same procedure is carried out with mCherry lacking  
196 the targeting peptide, which fails to result in cargo loading (right) and results in no detectable fluorescence after  
197 reassembly. B) NativePAGE analysis showing high molecular weight bands for assembled T4GALA via Coomassie blue  
198 staining (top) and fluorescence analysis of mNeon and mCherry (bottom).

## 199 Conclusion

200 From bionanoreactors to nanotherapeutic technologies, protein nanocage design presents  
201 significant opportunities across numerous research fields. While *de novo* protein cage design has led  
202 to several novel biomolecular tools,<sup>34</sup> increasing numbers of natural protein nanocompartments are  
203 being discovered that have been refined by evolution for biological activity and biocompatibility  
204 whilst also being amenable to rational engineering approaches.<sup>18,35</sup> The recent surge in encapsulin  
205 nanocompartment discovery and engineering further emphasizes this point.<sup>10,14,36</sup> Newly discovered  
206 protein cages provide an opportunity to create novel semi-synthetic hybrid compartments and  
207 bionanotechnological tools. For example, previous research has shown that disassembling and  
208 reassembling viral capsids or encapsulins requires extremes of pH<sup>7,37,38</sup> or salt concentration,<sup>39</sup>  
209 making these manipulations less applicable to biomolecular and biomedical research. In contrast,  
210 the T4GALA system described here is functional under milder conditions better suited for

211 conventional experimental procedures and potential biocatalysis or delivery applications. The  
212 T4GALA nanocage adds a novel dimension of control to encapsulin nanocages.

213 Via simple buffer exchanges within physiological pH and ionic strength ranges, the T4GALA system  
214 showcases the ability to undergo on-demand disassembly and reassembly. Structural analyses via  
215 cryo-EM confirm our overall design strategy by highlighting a lack of density for the rationally  
216 engineered disassembly trigger and an altogether more dynamic E-loop. The engineered protein  
217 cage also retains the ability of *in vivo* cargo loading via co-expression with targeting peptide-fused  
218 proteins of choice. Additionally, facile *in vitro* cargo loading under mild conditions represents a novel  
219 capability for encapsulin nanocages.

220 Potential applications of the T4GALA system include control over the unloading of relatively large  
221 encapsulated nanoreactor products, sequentially timed exposure of protected cargos to external  
222 molecules, *in vitro* encapsulation of enzymes that cannot be co-expressed with T4GALA, or even  
223 stoichiometric shuffling of nanocage components. In sum, the T4GALA system developed here  
224 represents a versatile addition to the growing encapsulin-based biomolecular engineering toolbox.

### 225 **Data Availability**

226 The determined structure has been deposited and the model was assigned the accession code PDB  
227 ID 7MH2. The final cryo-EM map was submitted to EMDB with the identifier 23834. All other data  
228 that support the findings of this study are available from the corresponding author upon request.

### 229 **Acknowledgements**

230 We gratefully acknowledge funding from the NIH (1R35GM133325). Research reported in this  
231 publication was supported by the University of Michigan Cryo-EM Facility (U-M Cryo-EM). U-M Cryo-  
232 EM is grateful for support from the U-M Life Sciences Institute and the U-M Biosciences Initiative.

233 Molecular graphics and analyses performed with UCSF ChimeraX, developed by the Resource for  
234 Biocomputing, Visualization, and Informatics at the University of California, San Francisco, with  
235 support from National Institutes of Health R01-GM129325 and the Office of Cyber Infrastructure and  
236 Computational Biology, National Institute of Allergy and Infectious Diseases.

### 237 **Author Contributions**

238 A.S.C., J.A.J., and T.W.G. designed the project. A.S.C. and T.W.G. designed the engineered protein cage.  
239 A.S.C. and J.A.J. conducted the laboratory experiments and transmission electron microscopy, while  
240 M.P.A. obtained and analyzed cryo-electron microscopy data. T.W.G. oversaw the project in its  
241 entirety.

### 242 **Competing Interests**

243 The authors declare no competing interests.

### 244 **Supporting Information**

245 Supporting Information containing methods and additional data and analyses is available and  
246 contains Figures S1-S9 and Tables S1-S2.

247

## 248 References

- 249 1 Cornejo, E., Abreu, N. & Komeili, A. Compartmentalization and organelle formation in  
250 bacteria. *Curr Opin Cell Biol* **26**, 132-138, doi:10.1016/j.ceb.2013.12.007 (2014).
- 251 2 Diekmann, Y. & Pereira-Leal, J. B. Evolution of intracellular compartmentalization. *Biochem J*  
252 **449**, 319-331, doi:10.1042/BJ20120957 (2013).
- 253 3 Azuma, Y., Edwardson, T. G. W. & Hilvert, D. Tailoring lumazine synthase assemblies for  
254 bionanotechnology. *Chem Soc Rev* **47**, 3543-3557, doi:10.1039/c8cs00154e (2018).
- 255 4 Khoshnejad, M., Parhiz, H., Shuvaev, V. V., Dmochowski, I. J. & Muzykantov, V. R. Ferritin-  
256 based drug delivery systems: Hybrid nanocarriers for vascular immunotargeting. *J Control*  
257 *Release* **282**, 13-24, doi:10.1016/j.jconrel.2018.02.042 (2018).
- 258 5 Ma, Y., Nolte, R. J. & Cornelissen, J. J. Virus-based nanocarriers for drug delivery. *Adv Drug*  
259 *Deliv Rev* **64**, 811-825, doi:10.1016/j.addr.2012.01.005 (2012).
- 260 6 Choi, S. H., Choi, K., Chan Kwon, I. & Ahn, H. J. The incorporation of GALA peptide into a  
261 protein cage for an acid-inducible molecular switch. *Biomaterials* **31**, 5191-5198,  
262 doi:10.1016/j.biomaterials.2010.03.016 (2010).
- 263 7 Li, Y. *et al.* Control of virus assembly: HK97 "Whiffleball" mutant capsids without pentons. *J*  
264 *Mol Biol* **348**, 167-182, doi:10.1016/j.jmb.2005.02.045 (2005).
- 265 8 Bae, Y. *et al.* Engineering Tunable Dual Functional Protein Cage Nanoparticles Using Bacterial  
266 Superglue. *Biomacromolecules* **19**, 2896-2904, doi:10.1021/acs.biomac.8b00457 (2018).
- 267 9 Lagoutte, P. *et al.* Simultaneous surface display and cargo loading of encapsulin  
268 nanocompartments and their use for rational vaccine design. *Vaccine* **36**, 3622-3628,  
269 doi:10.1016/j.vaccine.2018.05.034 (2018).
- 270 10 Williams, E. M., Jung, S. M., Coffman, J. L. & Lutz, S. Pore Engineering for Enhanced Mass  
271 Transport in Encapsulin Nanocompartments. *ACS Synth Biol* **7**, 2514-2517,  
272 doi:10.1021/acssynbio.8b00295 (2018).
- 273 11 Adamson, L. *et al.* Pore structure controls stability and molecular flux in engineered protein  
274 cages. *BioRxiv*, doi:<https://doi.org/10.1101/2021.01.27.428512> (2021).
- 275 12 Andreas, M. P. & Giessen, T. W. Large-scale computational discovery and analysis of virus-  
276 derived microbial nanocompartments. *BioRxiv*,  
277 doi:<https://doi.org/10.1101/2021.03.18.436031> (2021).
- 278 13 Lien, K. A. *et al.* A nanocompartment containing the peroxidase DypB contributes to defense  
279 against oxidative stress in *M. tuberculosis*. *bioRxiv*, 2020.2008.2031.276014,  
280 doi:10.1101/2020.08.31.276014 (2020).
- 281 14 Giessen, T. W. & Silver, P. A. Widespread distribution of encapsulin nanocompartments  
282 reveals functional diversity. *Nat Microbiol* **2**, 17029, doi:10.1038/nmicrobiol.2017.29 (2017).
- 283 15 McHugh, C. A. *et al.* A virus capsid-like nanocompartment that stores iron and protects  
284 bacteria from oxidative stress. *EMBO J* **33**, 1896-1911, doi:10.15252/embj.201488566  
285 (2014).
- 286 16 Contreras, H. *et al.* Characterization of a Mycobacterium tuberculosis nanocompartment and  
287 its potential cargo proteins. *J Biol Chem* **289**, 18279-18289, doi:10.1074/jbc.M114.570119  
288 (2014).
- 289 17 He, D. *et al.* Conservation of the structural and functional architecture of encapsulated  
290 ferritins in bacteria and archaea. *Biochem J* **476**, 975-989, doi:10.1042/BCJ20180922 (2019).
- 291 18 Giessen, T. W. *et al.* Large protein organelles form a new iron sequestration system with high  
292 storage capacity. *Elife* **8**, doi:10.7554/eLife.46070 (2019).
- 293 19 Nichols, R. J. *et al.* Discovery and characterization of a novel family of prokaryotic  
294 nanocompartments involved in sulfur metabolism. *bioRxiv*, 2020.2005.2024.113720,  
295 doi:10.1101/2020.05.24.113720 (2020).
- 296 20 Akita, F. *et al.* The crystal structure of a virus-like particle from the hyperthermophilic  
297 archaeon *Pyrococcus furiosus* provides insight into the evolution of viruses. *J Mol Biol* **368**,  
298 1469-1483, doi:10.1016/j.jmb.2007.02.075 (2007).

- 299 21 Altenburg, W. J., Rollins, N., Silver, P. A. & Giessen, T. W. Exploring targeting peptide-shell  
300 interactions in encapsulin nanocompartments. *Sci Rep* **11**, 4951, doi:10.1038/s41598-021-  
301 84329-z (2021).
- 302 22 Lau, Y. H., Giessen, T. W., Altenburg, W. J. & Silver, P. A. Prokaryotic nanocompartments  
303 form synthetic organelles in a eukaryote. *Nat Commun* **9**, 1311, doi:10.1038/s41467-018-  
304 03768-x (2018).
- 305 23 Tso, D. J., Hendrix, R. W. & Duda, R. L. Transient contacts on the exterior of the HK97  
306 procapsid that are essential for capsid assembly. *J Mol Biol* **426**, 2112-2129,  
307 doi:10.1016/j.jmb.2014.03.009 (2014).
- 308 24 Künzle, M., Mangler, J., Lach, M. & Beck, T. Peptide-directed encapsulation of inorganic  
309 nanoparticles into protein containers. *Nanoscale* **10**, 22917-22926, doi:10.1039/c8nr06236f  
310 (2018).
- 311 25 Jones, J. A. & Giessen, T. W. Advances in encapsulin nanocompartment biology and  
312 engineering. *Biotechnol Bioeng*, doi:10.1002/bit.27564 (2020).
- 313 26 Li, W., Nicol, F. & Szoka, F. C. GALA: a designed synthetic pH-responsive amphipathic peptide  
314 with applications in drug and gene delivery. *Adv Drug Deliv Rev* **56**, 967-985,  
315 doi:10.1016/j.addr.2003.10.041 (2004).
- 316 27 Kamiyama, D. *et al.* Versatile protein tagging in cells with split fluorescent protein. *Nat*  
317 *Commun* **7**, 11046, doi:10.1038/ncomms11046 (2016).
- 318 28 Moon, H., Lee, J., Min, J. & Kang, S. Developing genetically engineered encapsulin protein  
319 cage nanoparticles as a targeted delivery nanoplatfrom. *Biomacromolecules* **15**, 3794-3801,  
320 doi:10.1021/bm501066m (2014).
- 321 29 Romei, M. G. & Boxer, S. G. Split Green Fluorescent Proteins: Scope, Limitations, and  
322 Outlook. *Annu Rev Biophys* **48**, 19-44, doi:10.1146/annurev-biophys-051013-022846 (2019).
- 323 30 Ozawa, K. *et al.* Identification and characterization of thermostable glucose dehydrogenases  
324 from thermophilic filamentous fungi. *Appl Microbiol Biotechnol* **101**, 173-183,  
325 doi:10.1007/s00253-016-7754-7 (2017).
- 326 31 Kato, C. *et al.* Determination of pyrroloquinoline quinone by enzymatic and LC-MS/MS  
327 methods to clarify its levels in foods. *PLoS One* **13**, e0209700,  
328 doi:10.1371/journal.pone.0209700 (2018).
- 329 32 Lee, S. Y., Lee, J., Chang, J. H. & Lee, J. H. Inorganic nanomaterial-based biocatalysts. *BMB*  
330 *Rep* **44**, 77-86, doi:10.5483/BMBRep.2011.44.2.77 (2011).
- 331 33 Jordan, P. C. *et al.* Self-assembling biomolecular catalysts for hydrogen production. *Nat*  
332 *Chem* **8**, 179-185, doi:10.1038/nchem.2416 (2016).
- 333 34 Edwardson, T. G. W., Tetter, S. & Hilvert, D. Two-tier supramolecular encapsulation of small  
334 molecules in a protein cage. *Nat Commun* **11**, 5410, doi:10.1038/s41467-020-19112-1  
335 (2020).
- 336 35 Giessen, T. W. & Silver, P. A. Converting a Natural Protein Compartment into a Nanofactory  
337 for the Size-Constrained Synthesis of Antimicrobial Silver Nanoparticles. *ACS Synth Biol* **5**,  
338 1497-1504, doi:10.1021/acssynbio.6b00117 (2016).
- 339 36 Tracey, J. C. *et al.* The Discovery of Twenty-Eight New Encapsulin Sequences, Including Three  
340 in Anammox Bacteria. *Sci Rep* **9**, 20122, doi:10.1038/s41598-019-56533-5 (2019).
- 341 37 Huang, R. K. *et al.* The Prohead-I structure of bacteriophage HK97: implications for scaffold-  
342 mediated control of particle assembly and maturation. *J Mol Biol* **408**, 541-554,  
343 doi:10.1016/j.jmb.2011.01.016 (2011).
- 344 38 Rahmanpour, R. & Bugg, T. D. Assembly in vitro of *Rhodococcus jostii* RHA1 encapsulin and  
345 peroxidase DypB to form a nanocompartment. *FEBS J* **280**, 2097-2104,  
346 doi:10.1111/febs.12234 (2013).
- 347 39 Xie, Z. & Hendrix, R. W. Assembly in vitro of bacteriophage HK97 proheads. *J Mol Biol* **253**,  
348 74-85, doi:10.1006/jmbi.1995.0537 (1995).
- 349